Supporting Information

Stochastic detection of MPSA-gold nanoparticles by using a α-hemolysin nanopore equipped with a noncovalent molecular adaptor

Elisa J. Campos,[§][†] Colin E. McVey,[¥] and Yann Astier[§†]*

[§]Single Molecule Processes Laboratory, Instituto de Tecnologia Química e Biológica António Xavier, Universidade Nova de Lisboa, Av. da República, 2780-157 Oeiras, Portugal

[¥]Structural Virology Laboratory, Instituto de Tecnologia Química e Biológica António Xavier, Universidade Nova de Lisboa, Av. da República, 2780-157 Oeiras, Portugal

Corresponding author:

*Elisa J. Campos, PhD.

Single Molecule Processes Laboratory, Instituto de Tecnologia Química e Biológica António Xavier, Universidade Nova de Lisboa, Av. da República, 2780-157 Oeiras, Portugal.

E-mail: elisacampos@itqb.unl.pt; elisajcampos@yahoo.com.

Fax: +351 21 441 12 77.

Present Addresses: Institute for Biomedical Imaging and Life Sciences (IBILI), Faculty of Medicine, University of Coimbra, 3000-548 Coimbra, Portugal.

Table of Contents

SI Text – Results and Discussion: Part 1 - Interaction of γCD with WT-αHL and M113N mutant nanopores …… S-4

SI Text – Results and Discussion: Part 2 - Interaction of MPSA NPs with WT-αHL and M113N mutant nanopores …… S-11

SI Text – Experimental Section: Data Analysis …… S-15

SI Text – Experimental Section: Statistical Analysis …… S-15

Figure S1. Molecular models of the Staphylococcal WT-αHL and M113N mutant nanopore …… S-18

Figure S2. Structure of cyclodextrins …… S-19

Figure S3. Molecular model of MPSA NP …… S-20

Figure S4. Representative ionic current traces for the interaction between MPSA NPs and the α-HL pore coupled with γCD …… S-21

Figure S5. Schematic representation of the rationale for the comparison between the blockade caused by MPSA NPs in the protein nanopore and in the nanopore:γCD complex …… S-22

Figure S6. Comparison of the noncovalent binding of γCD to M113N and WT-αHL nanopores …… S-23

Figure S7. Experimental voltage-dependency …… S-24

Figure S8. Protein nanopore-dependency of the current blockade during the interaction with γCD …… S-25

Figure S9. Protein nanopore-dependency of the dwell time during the interaction with γCD …… S-26

Figure S10. Protein nanopore-dependency of current blockade and of dwell time during the interaction with MPSA NPs …… S-27

Figure S11. Scatter plots of blockade duration *versus* the current blockade for the interaction of MPSA NPs with the M113N mutant and with the WT-αHL nanopores …… S-28

Table S1. Current blockade percentage and dwell time values for the interaction of MPSA NPs with the protein nanopores and γCD ……..……..…..…….. S-29

Table S2. Ionic current, current blockade and dwell time values for the interaction of γCD with protein nanopores ……..…… S-31

Table S3. Diameter of WT-αHL and M113N β barrels …….……..…..……. S-32

Table S4. Current blockade percentage and dwell time values for the interaction of MPSA NPs with the M113N mutant and WT-αHL nanopores ……...…….. S-32

Table S5. Pearson correlation coefficients for the relationship between the current blockade and the dwell time ……...……..…….. S-33

References …….....…….……. S-34

Results and Discussion

Interaction of γCD with WT-αHL and M113N mutant nanopores

It was shown previously that βCD binds in the stem, close to the aforementioned constriction region, in a section of the β barrel that comprises (from the *trans* side) the amino-acid residues Met113, Lys147 and Glu111.[1] Due to its location, Met113 was thus highlighted as a critical residue for the binding of βCD within the αHL nanopore. The αHL nanopore appears to possess a remarkable tolerance for site-directed mutagenesis and can therefore be engineered[2] with atomic precision. This allowed researchers to make a range of Met113-mutants, replacing Met113 with each of the other naturally occurring amino acids (one at a time). The aim was to isolate Met113 mutants in which the residence time (dwell time) of βCD within the αHL nanopore was increased.[3] One of the members of the tight-binding class is the M113N mutant protein nanopore in which the Met113 residue was replaced with an asparagine,[3] and whose binding interactions and high-resolution X-ray crystallographic structure are already known.[4]

Single-channel electrical recordings in planar lipid bilayers were carried out in 2 M KCl buffered with10 mM HEPES (pH 8.0). Under these conditions, stable and uniform single-channel current recordings of long durations could be made for the open state at both negative and positive transmembrane potentials and with both WT-αHL and M113N mutant nanopores, as described previously.[5] When a single M113N mutant protein nanopore was introduced into a lipid bilayer, from the *cis* chamber, we measured an ionic current of 151 $\pm$ 4 pA, at +80 mV (N = 104), and of -119 $\pm$ 3 pA, at -80 mV (N = 90) which is slightly smaller than that of the WT-αHL nanopore (154 $\pm$ 2 pA, N = 137, and -128 $\pm$ 2 pA, N = 49, respectively) under the same conditions (Table S2), in agreement with previous studies.[3, 6]

In order to study the interaction of γCD with each protein nanopore, the CD was added to the *trans* chamber, since it was shown previously that no interaction occurs when CD is added to the *cis* side of the nanopore/lipid bilayer.[7] When 20 μM γCD was added to the *trans* side of a protein nanopore, inserted in a lipid bilayer, the ionic current was reduced in a partial and reversible way from the value recorded for the open nanopore (open nanopore current; I_O) to the γCD occupied nanopore current (I_B). At +80 mV, the ionic current was reduced from 151 $\pm$ 4 pA to 50 $\pm$ 2 pA and from 154 $\pm$ 2 pA to 49 $\pm$ 2 pA, while γCD was bound to the M113N and WT-αHL nanopores, respectively. Accordingly, the ionic current blockade, defined as $(I_O - I_B)/I_O$, expressed as a percentage, was ~67% and ~68%, respectively. At -80 mV smaller blockades were measured: from -119 $\pm$ 3 pA to -51 $\pm$ 1 pA (blockade ~58%, M113N) and from -128 $\pm$ 2 pA to -49 $\pm$ 1 pA (blockade ~60%, WT-αHL) (Table S2). Current blockade histograms revealed only one current blockade level for the interaction of γCD with each of the protein nanopores (a representative histogram is shown as an insert in Figure S6.A), suggesting that there is only one binding site for γCD within the stem of the protein nanopore, accessible from the *trans* side of the lipid bilayer,[7, 8] in 2 M KCl buffered with 10 mM HEPES, pH 8.0.

Figure S6.A shows the current versus voltage *(I-V)* curves for M113N and WT-αHL nanopores with and without γCD recorded in symmetrical salt concentrations (2 M KCl in both *cis* and *trans* reservoirs). The apparent linearity of the *I-V* curves would lead to the conclusion that the conductance of both protein nanopores does not change markedly throughout the voltage range from -100 mV to +100 mV. However, plotting the conductance ($G = I/V$) as a function the applied transmembrane potential reveals that the conductance of both M113N and WT-αHL nanopores is voltage dependent and increases continuously from -100 to +100 mV[9] (Figure S6.B). At positive potential,

conductance is higher than at negative potential. This difference in conductance is typical for an asymmetric nanopore, such as the αHL nanopore. The smaller conductance at negative potential is due to the decrease in cation (K^+) current, while the anion (Cl^-) current remains almost constant between negative and positive potentials.[6] This difference between cation and anion selectivity makes the αHL nanopore weakly anion selective.[5] It was shown that the anion selectivity of the M113N nanopore is higher than for WT-αHL nanopore. Molecular dynamics[6, 10] and crystallographic[4] studies revealed that this difference can be related to the different orientations of the seven positively charged Lys147 residues in the constriction region of the protein nanopore (Figure S1). Whereas in the WT-αHL nanopore, Lys147 residues are pointing upwards (towards the *cis* opening), in the M113N mutant nanopore, they are pointing slightly downwards (towards the *trans* opening) but are almost perpendicular to the channel axis, which results in a narrower constriction at the Lys147 ring and, thus, creates a very strong electrostatic field in this region of the nanopore.[26, 27] Accordingly, in the M113N mutant nanopore, the overall ionic current is slightly reduced and, in particular, the cationic current is reduced, particularly at negative potential, as shown in Figure S6.B.

The binding of γCD to M113N and WT-αHL nanopores reduces the conductance of the nanopores,[11] in a voltage independent manner (Figure S6.B). The ion selectivity depends on the nanopore dimensions and spatial distribution of charges at the entrance to and within the nanopore lumen. A wide nanopore shows almost no selectivity as an ion in such a nanopore interacts primarily with water and other ions, rather than with the nanopore residues. Conversely, narrow nanopores (d = 0.3-0.4 nm) show a markedly higher charge selectivity and also a considerable discrimination among ions of the same charge, due to the dehydration of the ion entering the nanopore. In between these

extremes of nanopore sizes are the mid-sized nanopores (d = 0.7-0.8 nm), which show high charge selectivity, but only a low selectivity among ions of the same charge.[12] The αHL nanopore is considered a ‘‘wide nanopore’’[5] since the narrow internal diameter is ~1.4 nm and shows weak charge selectivity (Figure S1).[13] Lodging γCD in the stem region introduces a mid-sized constriction (γCD internal diameter 0.75-0.83 nm;[14, 15] Figure S1.A), sufficient to admit the passage of a hydrated ion, as shown by the reduction in conductance. This narrowing of the nanopore is also responsible for the increase in anion selectivity.[11, 16] The reduction in conductance is less pronounced when γCD interacts with the M113N nanopore (Figure S6.B). We hypothesize that the effect of γCD on the conductance of the M113N nanopore is less pronounced as the change in internal diameter is not as great. As described above, the Lys147 ring in the M113N mutant adopts an orientation that is more perpendicular to the channel axis and thus reduces the size of the constriction. The decreases in conductance observed, when βCD or γCD interact with the M113N mutant nanopore were similar (data not shown). βCD has a narrower internal diameter (0.60-0.65 nm;[14, 15] Figure S1.A) and therefore, it was expected to have a slightly greater effect than γCD on the conductance of the M113N nanopore,[11] based on the anticipated decrease in ionic current (mainly the cationic, K^+ current).[6] The lack of difference between the conductances observed for βCD and γCD suggest that the ionic current is mostly carried by the Cl^- anions.[9] The interaction between βCD and the M113N nanopore also makes the nanopore more anion selective[6, 11] because βCD reduces the shielding, by local ions and water, of the strong electrostatic field induced by the nearby ring of seven Lys147 residues.[6]

The current-voltage relationship of the αHL ion channel is known to be nonlinear and rectifying,[17] that is to say that absolute values of the current at a positive voltage (I_{+V}) and at the corresponding negative voltage (I_{-V}) are different.[9] Rectification can be

represented quantitatively as the ionic current rectification (ICR) ratio[18] or the current asymmetry factor,[9] defined as $(I_{+V})/(I_{-V})$. The ICR ratio for M113N and WT-αHL nanopores increases with the increase in the applied transmembrane potential (Figure S7.A), as observed in other studies.[19] At negative potentials, the current is carried mostly by Cl^-, whereas at positive potentials, the fractional current carried by K^+ ions increases with the applied potential,[9, 10] making the ionic current more voltage-dependent at positive potentials. In the case of symmetric currents, the cations are expected to carry a minor fraction of the current. In contrast, the higher degree of rectification indicates that the cations contribute significantly to the ionic current.[9] Accordingly, the cationic current has a greater effect on current rectification than the anionic current. That is to say, a more anion selective nanopore, such as M113N, in which the cationic current changes more noticeably from negative to positive potentials, will be expected to be more rectifying. This rationale is in agreement with Figure S7.A. Figure S7.A also shows, once again, that γCD increases the anion selectivity of the protein nanopore, the anionic current becomes prevalent and, thus the total (or net) ionic current is symmetric.

Figure S7.B shows the voltage-dependency of the residual current, defined as the γCD occupied nanopore current (I_B) divided by the open nanopore current (I_O), when a γCD molecule is lodged in the protein nanopore. Higher residual current values were obtained at negative applied potentials,[3] resulting in a reduced current blockade, as shown before in Table S2. At negative potential, the anionic current (the predominant current) flows from the *trans* side to the *cis* side, favoring the interaction of γCD (added to the *trans* side) with the nanopore lumen. Accordingly, lower residual current would be expected at negative potentials. However, due the asymmetry and anion selectivity of the αHL nanopores, the K^+ current is naturally lower, at negative potential, and,

therefore, the effect of the γCD on the overall ionic current will not be as striking as at positive potential.

For a significance level of 0.05, statistically significant differences exist between the two different nanopores with regard to positive applied potential ($p < 0.001$), as determined by an independent t-test (Figure S8). The interaction of γCD with the M113N nanopore causes smaller current blockades than are caused by the interaction of γCD with the WT-αHL nanopore. As mentioned above, this effect on current blockade can be understood as the influence that γCD has in ion current *per se*. Thus, γCD decreases the total ion current more significantly in the WT-αHL nanopore. This result also suggests that the change in anion selectivity is more noticeable when γCD is accommodated in the WT-αHL nanopore than in the M113N nanopore.

The molecular bases for the interactions of βCD with selected αHL mutants (*i.e.*, M113N, M113F, M113V, M113A, and M113E mutants) have already been described.[4, 20] The interaction of βCD with the WT-αHL nanopore occurs mainly via van der Waals interactions with Met113 residues. Hydrogen bonds between the primary (O_6) or secondary (O_2 and O_3) hydroxyl groups of βCD (donors) and the hydroxyl groups of Thr145 (5 out of 7 subunits) and Thr115 (2 out of 7; acceptors) are also believed to contribute considerably to the stabilization of βCD in the WT-αHL nanopore.[20] Concerning the M113N mutant nanopore, since the side chain of the asparagine residue is polar, it can act as both hydrogen bond donor and acceptor. In fact, the Met113Asn residues act as hydrogen bond donors to the O_5 and O_6 positions of βCD;[20] while at the same time, the primary hydroxyl groups of βCD act as donors and form hydrogen bonds with the Met113Asn carbonyl groups. The secondary hydroxyl groups in the βCD are also able to form hydrogen bonds with Lys147 (3 out of 7).[4, 20] To further increase the

stability of the βCD in the M113N nanopore, hydrogen bonds are also formed between βCD and Thr145 and Thr115, as described above for the WT-αHL nanopore.[20]

Previous studies with hepta-6-sulfato-βCD,[21] led to the conclusion that large CDs, such as γCD, become lodged near to residue Asn139 in the WT-αHL β barrel.[19] Therefore, γCD and βCD are expected to bind in different regions of the WT-αHL nanopore. Furthermore, the authors also assumed that hepta-6-sulfato-βCD should be lodged in the lumen with the sulfated face oriented toward the *trans* entrance. Since the chemical modification was made on the primary hydroxyl groups,[11] we can conclude that large CDs interact with the WT-αHL β barrel in the same orientation in which βCD interact with the M113N β barrel.[4] However, when comparing the β barrel's inner diameters with the outer diameters of βCD and γCD, different conclusions are reached. The internal diameters of the β barrels in WT-αHL and M113N, at positions aligned with Leu135 and Asn139 residues (Table S3), were obtained using the measurement wizard from PyMOL[22] and the appropriate PDB accessions codes (7AHL,[13] for WT-αHL; 3M4D,[4] for M113N mutant).

Thus, taking into account the outer diameter of γCD (1.75 $\pm$ 0.04 nm),[14] it seems unlikely that γCD would be able to pass beyond Leu135 and form further interactions with Asn139. On the contrary, βCD (outer diameter 1.54 $\pm$ 0.04 nm)[14] is clearly able to traverse up the β barrel to the constriction region, forming the interactions described earlier. This rationale makes us believe that γCD is unlikely to interact with the residues in the constriction region of the protein nanopore (namely, Lys147 and Met113 or Met113Asn). Accordingly, the effect that γCD has on WT-αHL and on M113N ion currents must be due only to its influence on anion selectivity, as described above.

It can be further concluded that the interaction of γCD with the WT-αHL nanopore is generally of longer duration than the interaction with the M113N nanopore.

This difference is statistically significant at +60 mV and +100 mV ($p < 0.001$) according to a Mann-Whitney U test, as depicted in Figure S9.

The electroosmotic flow of water through an anion selective nanopore, from the *cis* to the *trans* side of the bilayer, is enhanced as the applied positive potential is increased.[23] Since the M113N nanopore is more anion selective that the WT-αHL nanopore, we consider that the increase of the electroosmotic flow of water through the M113N nanopore with the increase of the applied potential, is more noteworthy. Hence, the interaction of γCD (added in the *trans* side of the lipid bilayer) is expected to be hampered and, thus, shortened, with the M113N nanopore, and as the applied potential increases.

Interaction of MPSA NPs with WT-αHL and M113N mutant nanopores

When added to the *cis* side of the lipid bilayer, containing a previously inserted single WT-αHL or M113N mutant nanopore, MPSA NPs enter the lumen of the protein nanopore and cause a reversible reduction in ionic current flowing through the nanopore. The hydrodynamic diameter of MPSA NPs was estimated, by analytical ultracentrifugation (AUC), to be between 3.90 nm and 6.21 nm.[24] The differences in size populations were partly due to inherently stochastic nucleation processes during NP synthesis and probably also due to the fact that ligand compositions were different in each synthesis and their energetics of absorption to the gold cluster surface during nucleation and growth would be subtly different. The dynamics of such processes are unknown currently. Furthermore, the relative proportion of different sizes and their spread are slightly random and the part that is not random is not quite understood yet. Despite the fact that the αHL protein nanopore *cis* opening diameter (2.8 nm; Figure S1) is smaller than the hydrodynamic diameter of the MPSA NPs, we assume that the NP

diameter estimated by AUC includes a small hydration shell and also that the ligands possess a degree of flexibility and thus can bend. We also assume that the interactions recorded throughout this study have occurred within the nanopore cavity, and that the interactions at the *cis* opening of the nanopore (if they occur) are invisible or not accurately measured at our recording resolution.[24]

The interaction of MPSA NPs (10 μg mL^{-1}) with WT-αHL and M113N mutant nanopores, in 2 M KCl buffered with 10 mM HEPES at pH 8.0, produced well-defined and statistically significant ($p < 0.001$, as determined by a paired t-test) populations of current blockades, for each applied transmembrane potential (Table S4). The number of populations of current blockades increases for higher applied transmembrane potentials. We believe that these current blockade levels/populations may be associated with: 1) MPSA NPs with different chemical and/or physical characteristics undergoing different interactions with the protein nanopore, thus generating different interaction profiles (in terms of current blockades and dwell times); 2) simply different interaction profiles between MPSA NPs and the protein nanopore.

Larger current blockades may be associated with stronger interactions within the protein cavity, namely, with the constriction region, and/or with higher stabilization of the NPs inside the cavity due to a shift in the balance between attractive and repulsive forces. These different profiles may be enhanced by, or may actually arise as a consequence of higher applied potentials. Besides, increasing applied potential improves the resolution of this methodology,[25] so we argue that these differences are also likely to be better distinguished as the applied potential increases.

We have also observed that MPSA NPs cause statistically significant higher current blockades ($p < 0.001$, as determined by an independent t-test), when interacting with the M113N mutant nanopore, except in the case of the fourth population at +100

mV (Figure S10). Since the M113N nanopore was shown to be more anion selective than the WT-αHL nanopore, this would favor an interaction with negatively charged MPSA NPs, allowing for stronger current blockades to occur. Similarly, longer dwell times were observed with the M113N mutant nanopore compared to the WT-αHL nanopore (Figure S10), being statistically significant ($p \geq 0.05$, as determined by a Mann-Whitney U test) except at +80 mV (first and third populations) and at +100 mV (fourth population).

Table S4 also shows that dwell time increases with the current blockade, under all experimental conditions. This relationship can be visualized in Figure S11, where we display semilog scatter plots of dwell time *versus* current blockade for the interaction between MPSA NPs and the M113N mutant nanopore and between MPSA NPs and the WT-αHL nanopore, at applied potentials of +60 mV, +80 mV, and +100 mv, highlighting the different populations discussed above.

The strength of the relationship between the current blockade and the dwell time was evaluated by the Pearson product-moment correlation coefficient (or Pearson correlation coefficient, for short), denoted by r (Table S5). The Pearson correlation coefficient values highlight that a positive correlation exists between the current blockade and the dwell time of each population, meaning that as one variable increases or decreases in value, the second variable also increases or decreases in value. The strength of the relationship between the two variables is mainly weak ($0.2 < r < 0.4$) or moderate ($0.4 < r < 0.7$). This means that changes in one variable are weakly or moderately correlated with changes in the second variable. Further, since statistically significant ($p < 0.05$ and $p < 0.01$) correlations are observed between the two variables, we concluded that increases or decreases in one variable do significantly relate to increases or decreases in the second variable.

Finally, Table S5, also shows that current blockades and dwell time increase with the applied potential. The electroosmotic flow of water through both slightly anion selective M113N and WT-αHL nanopores, from the *cis* to the *trans* side of the bilayer, is expected to increase as the applied positive potential increases, thus increasing current blockade and dwell time.[23]

Experimental Section

Data Analysis

In the initial analysis, current blockade percentage values were expressed as the peak values of the Gaussian fits to the current blockade percentage histograms (bin width 0.5), as determined using Clampfit (Molecular devices, version 10.3). Dwell times were determined by a single exponential fit by performing the Chebyshev procedure on the dwell time histograms (bin width according to Shimazaki and Shinomoto, 2007)[32] as determined by Clampfit version 10.3. Here, we presented the current blockade percentage values as the mean $\pm$ standard deviation (SD), as determined using SPSS (SPSS Statistics for Windows, IBM Corp, version 20.0, Armonk, NY), since they were in good agreement with the peaks of the Gaussian fit to the current blockade percentage histograms. Dwell time values are always represented by the median as determined using SPSS, because we found that it was also in good agreement with the exponential fitting. The dwell time frequency distributions were positively skewed (skewness coefficient > 0) and leptokurtic (kurtosis coefficient > 3; data not shown). When dealing with skewed data, as in this case, the median is the more robust measure of central tendency because it is less affected by the skewed values.[30, 31] Therefore, in order to be consistent, in cases where both current blockade and dwell values were analysed (*e.g.*, Table S1), median was chosen as central measure.

Statistical Analysis

The statistical analysis was performed using SPSS. The Shapiro-Wilk test was used for assessing normality of data. This test is more appropriate for small sample sizes (< 50 samples), but can also handle sample sizes as large as 2000. For data not normally distributed, the Central Limit Theorem was considered for large sample sizes ($N > 30$).

For smaller samples, skewness coefficient was determined and normality was assumed if values were between -1.96 and +1.96.

In the case of normally distributed data, the Levene's test was then used to test the assumption of homogeneity of variance. If the assumption of homogeneity of variance was met, the parametric one-way analysis of variance (ANOVA) statistic was used to determine whether there were any significant differences between the two or more subgroups. In the groups in which any significant differences were found, a post-hoc analysis was performed using pairwise Gabriel's tests, to determine which subgroups differed. Gabriel's test was used for post-hoc analysis of one-way ANOVA when the groups are of unequal sizes. If the equal variance assumption was invalid, the Welch test was used instead. The Welch test is more powerful and more conservative for this purpose. In this case, the post-hoc analysis was based on a Games-Howell test. Differences between variables were analysed using paired t-tests whereas an independent t-test was used to compare the means between two groups on the same variable.

Distributions that deviated from normality were evaluated using non-parametric tests. Thus, the Kruskall-Wallis test was used to determine whether there were any significant differences in median values for a variable with more than two independent sample subgroups. Since nonparametric tests do not include post-hoc testing, a series of Mann-Whitney U tests was performed to ascertain which pairs of groups differ significantly from one another. The Mann-Whitney U test was used to assess differences between two independent samples. Differences between groups were considered significant for p-value < 0.05.[33, 34]

In order to describe data, one needs to assign a value or measure to the central tendency (or central location), and to include a measure of spread or dispersion (which

describes the variability in the sample). Normally distributed data were represented by mean $\pm$ standard deviation (SD). Concerning skewed, non-normal and/or data with outliers, the median and interquartile range were chosen as measure of central tendency and spread, respectively, because these measures are not strongly affected by the skewed values or outliers. Here, the interquartile range is the difference between the first and the third quartile (also called the 25^{th} and the 75^{th} percentile, respectively).[30, 31] Pearson's correlation coefficient was used to measure relationships between variables.

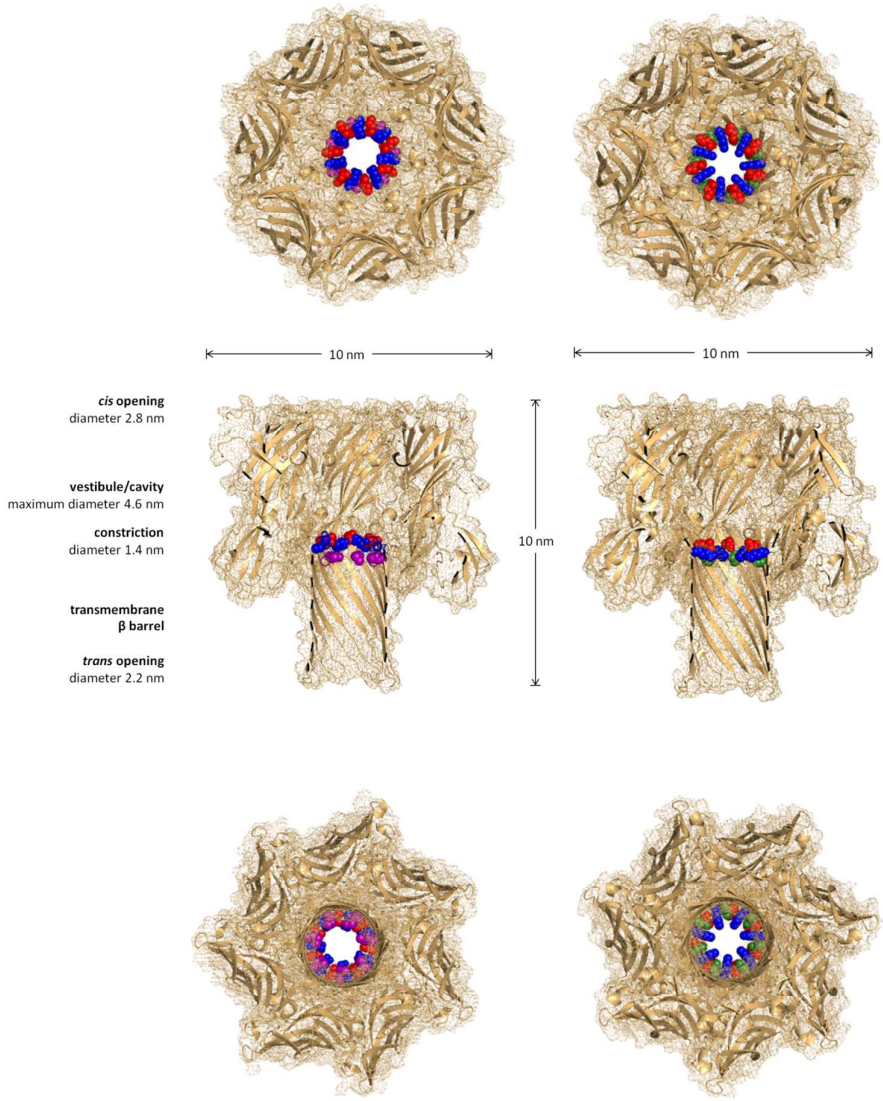

Figure S1. Molecular models of the (left panel) Staphylococcal wild-type α-hemolysin (WT-αHL) protein nanopore and (right panel) M113N mutant nanopore. Figures illustrate the top view (top panel), the cross-sectional view (middle panel), and the bottom view (bottom panel) of the mushroom-shaped heptamer. The location of the ion pair, Glu111-Lys147 at the constriction region, is coloured in red and blue (Glu and Lys respectively). The locations of Met113 (WT-αHL, left panel) and Met113Asn (mutant, right panel are coloured in purple and green, respectively. Each of these residues is represented by its side chain, for simplicity, in a sphere model. The backbone of the protein nanopore is coloured in "lightorange", in a mesh and cartoon model. Figures were rendered from PDB accession codes 7AHL[13, 26] (WT-αHL) and 3M4D[4] (M113N mutant) using PyMOL software.[22]

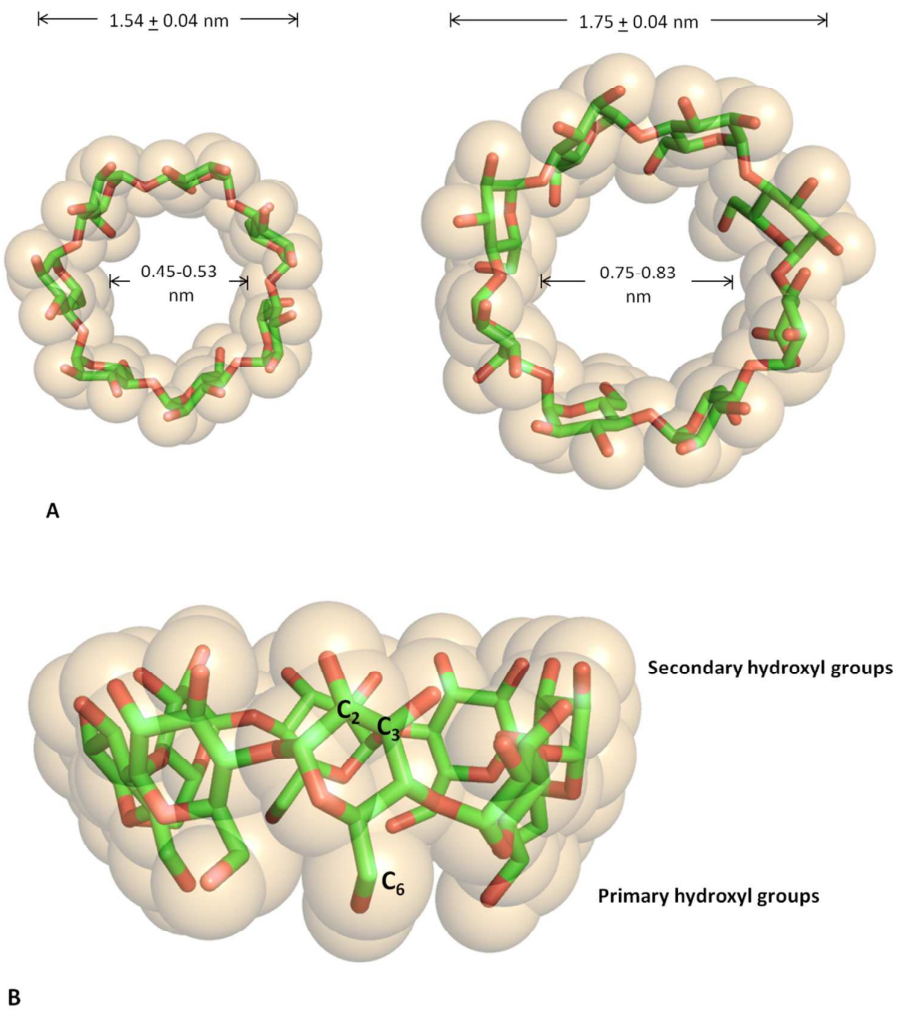

Figure S2. Structure of cyclodextrins. (**A**) Stick and sphere models of (left side) β-, and (right side) γ-cyclodextrin viewed from the wide end, showing the approximate molecular dimensions.[3] (**B**) General side view of a cyclodextrin, showing a hollow truncated cone, where the C_6 primary hydroxyl groups are at the narrower end and the C_2 and C_3 secondary hydroxyl groups are at the wider one. Figures were rendered from Protein Data Bank (PDB) accession codes 3M4E[4] (β-cyclodextrin) and 1P2G[27] (γ-cyclodextrin) using PyMOL software.[22]

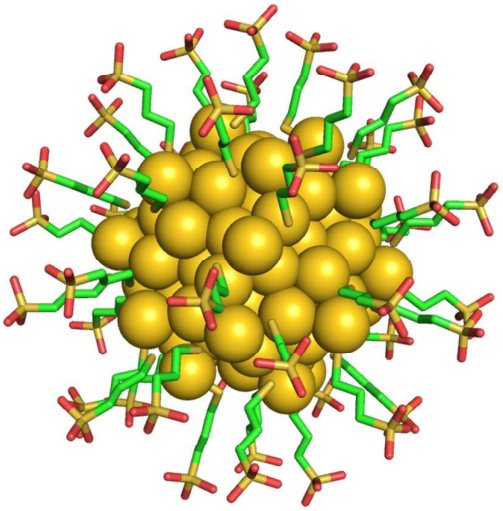

Figure S3. Molecular model showing the MPSA NP, with gold core and MPSA ligands.[28] This model is based on the gold core of the X-ray structure of *p*-mercaptobenzoic acid (p-MBA)-modified gold NP,[29] since both cores had similar average dimensions. (see reference[28], for details)

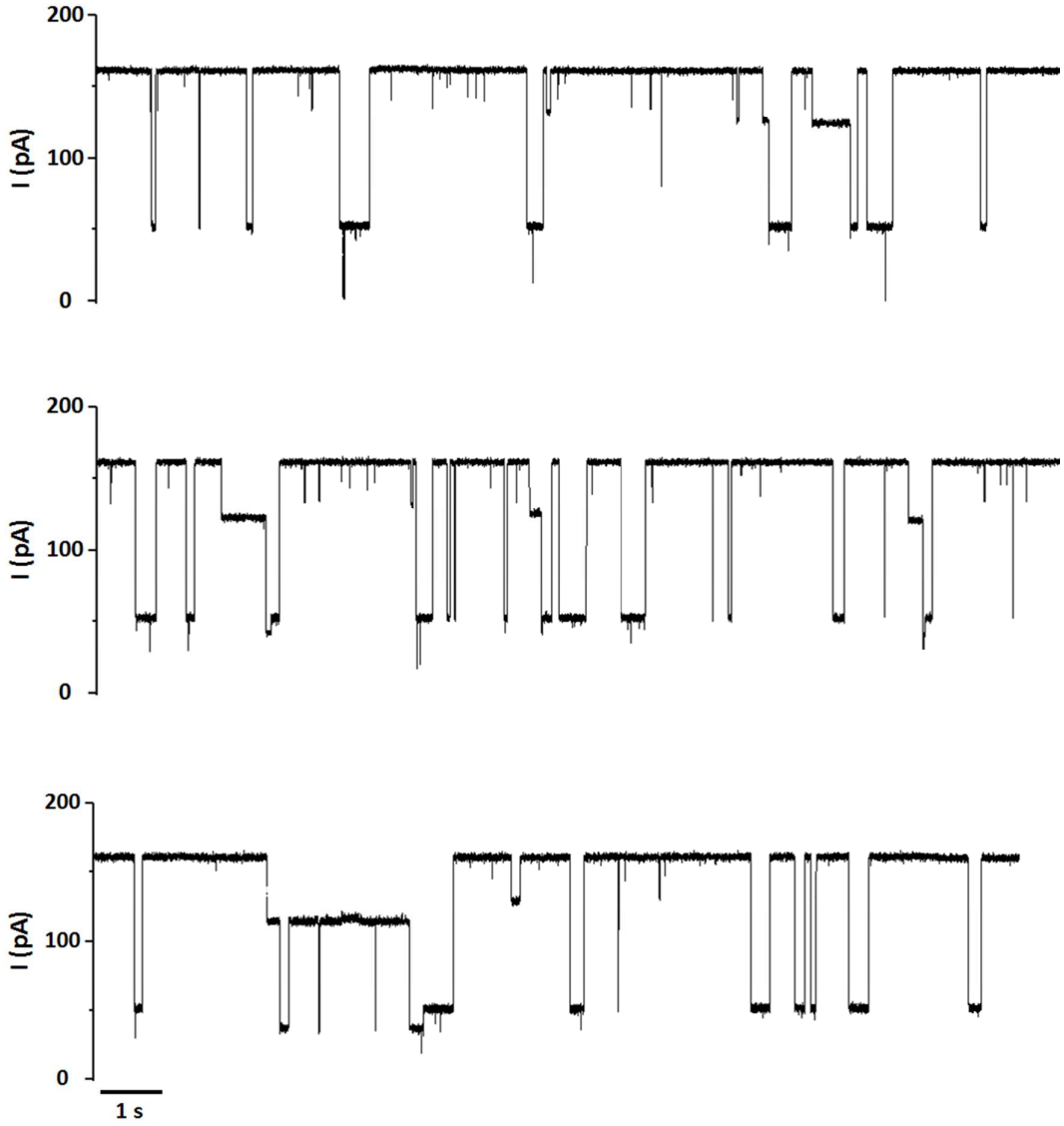

Figure S4. Representative ionic current traces showing the reversible interactions between MPSA NPs and the α-HL pore coupled with γCD. The different type of events are observed randomly (type of events are depicted in Figure 1). The experiments were performed at +80 mV in 2 M KCl buffered at pH 8.0 (10 mM HEPES), with 20 μM γCD in the *trans* compartment, and with 10 μg mL^{-1} MPSA NPs in the *cis* compartment.

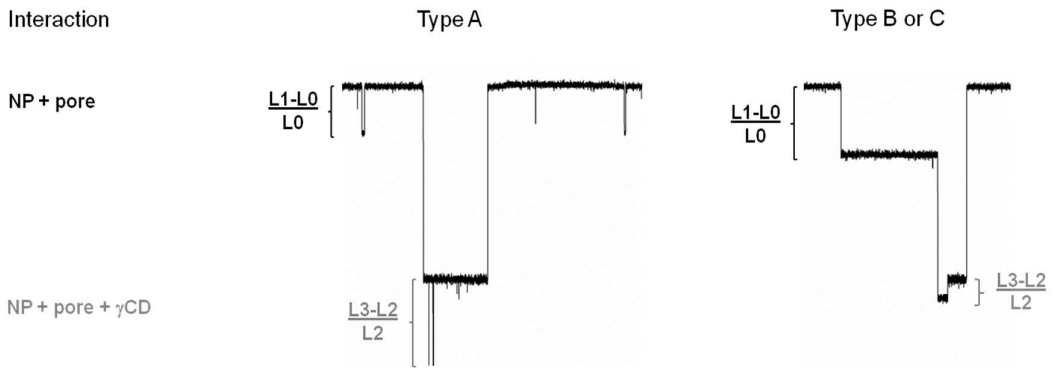

Figure S5. Schematic representation of the rationale for the comparison between the blockade caused by MPSA NPs in the protein nanopore (NP + nanopore) and in the nanopore:γCD complex (NP + nanopore + γCD), for type A, B, and C events. L0, L1, L2, and L3, denote the open nanopore state and the three blockade levels (level 1, level 2, and level 3) observed, respectively (see main text for details).

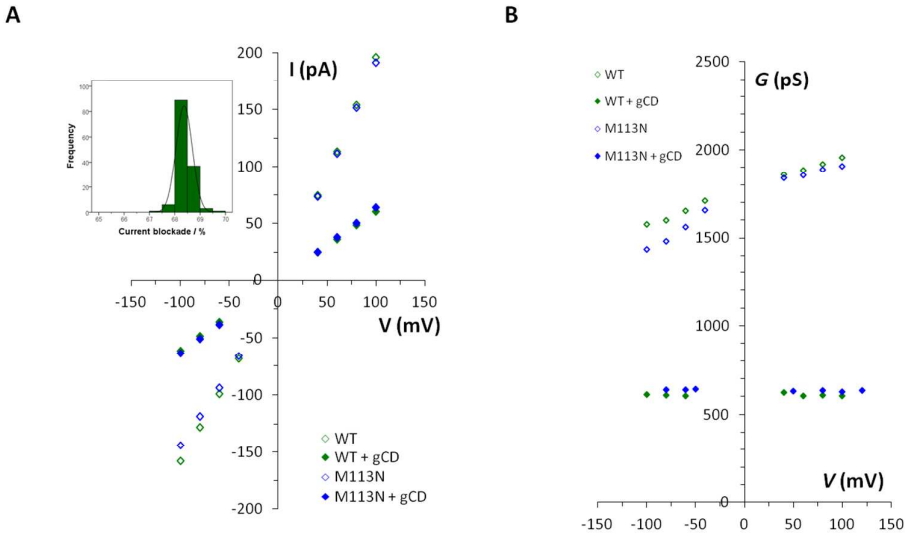

Figure S6. Comparison of the noncovalent binding of γCD to M113N and WT-αHL nanopores, determined by single electrical channel recording. Single-channel (**A**) *I-V* curves and (**B**) conductance values for the M113N and WT-αHL nanopores with and without γCD. Also included in panel (A) is a representative current amplitude histogram from a recording, at +80 mV, showing the current blockade values ($(I_O - I_B)/I_O$, expressed as a percentage) for the interaction of γCD with the WT-αHL nanopore. SD error bars were omitted, for simplicity (see Table S2, for details). Data was recorded under symmetrical salt conditions in buffer containing 2 M KCl, 10 mM HEPES, pH 8.0 (on both the *cis* and *trans* sides).

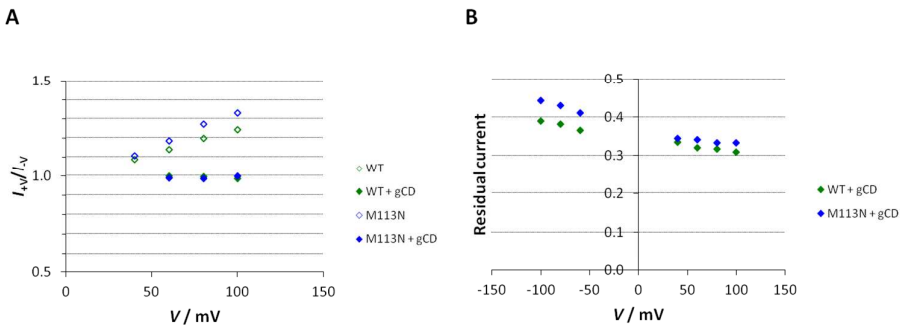

Figure S7. Experimental voltage-dependency. (**A**) current asymmetry factor $(I_{+V})/(I_{-V})$ and (**B**) residual current of conductance for M113N and WT-αHL nanopores with and without γCD. Experiments were performed in 2 M KCl, buffered with 10 mM HEPES, at pH 8.0, in the presence of 20 μM γCD *trans* added.

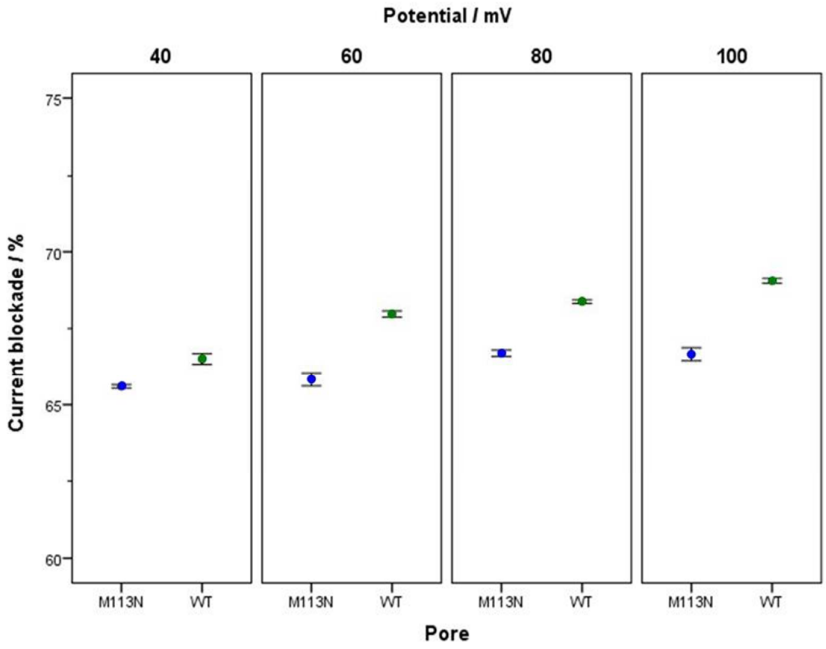

Figure S8. Protein nanopore-dependency of the current blockade during the interaction with γCD, at several applied potentials. Values are displayed as means and the errors given are standard deviations from 24-137 individual events observed with 4-5 independent nanopores. Data were collected at different applied potentials in 2 M KCl, 10 mM HEPES, pH 8.0, with 20 μM γCD in the *trans* chamber.

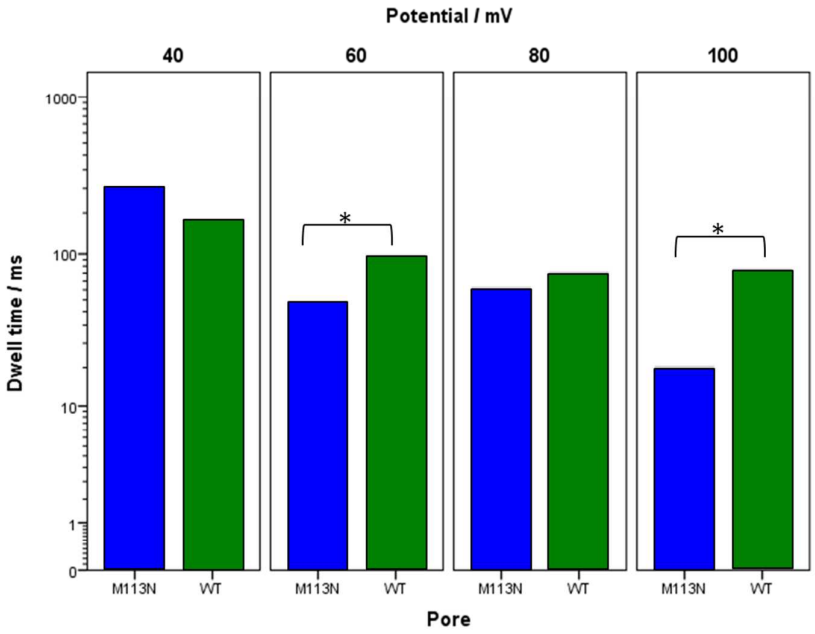

Figure S9. Protein nanopore-dependency of the dwell time during the interaction with γCD, at several applied potentials. Values are displayed as median from 24-137 individual events recorded with 4-5 independent nanopores. Data were collected at different applied potentials in 2 M KCl, 10 mM HEPES, pH 8.0, with 20 μM γCD in the *trans* chamber.

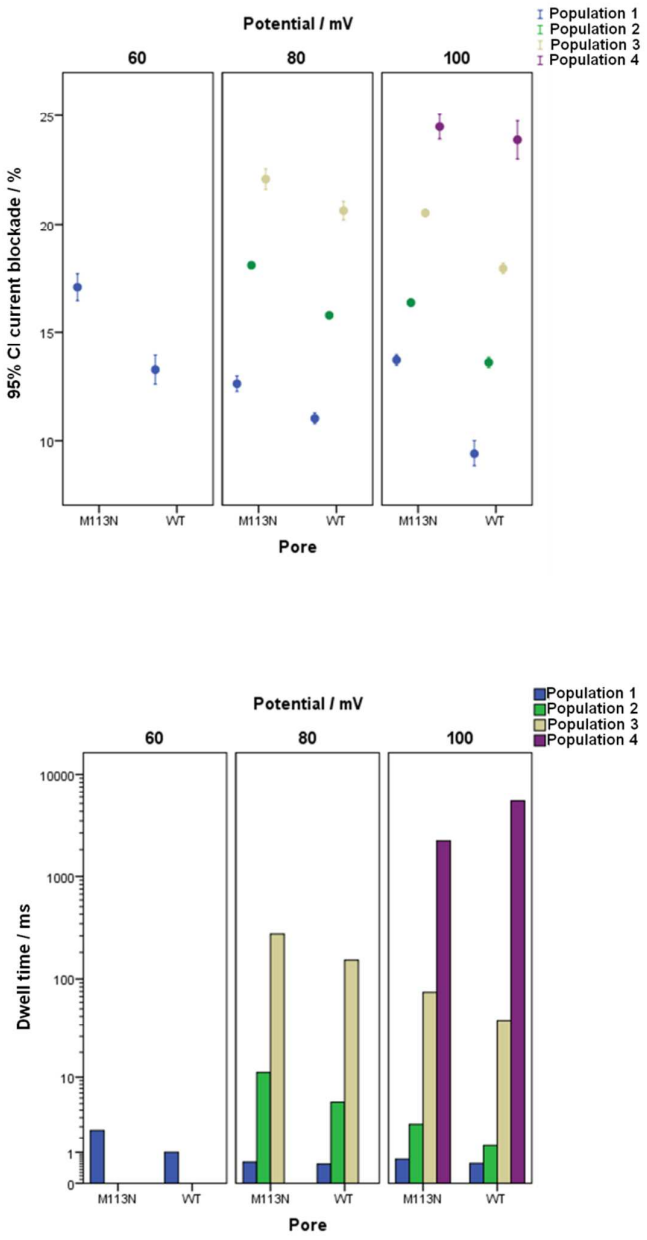

Figure S10. Protein nanopore-dependency of (top panel) current blockade and of (bottom panel) dwell time during the interaction with MPSA NPs, at several applied potentials. Current blockade values are the mean ± 95% confidence interval (CI) and dwell time values are the median obtained from 18-156 individual events in 4-5 independent nanopores (see Table S4, for details). Data were collected at different applied potentials in 2 M KCl, 10 mM HEPES, pH 8.0, with 10 μg mL^{-1} MPSA NPs in the *cis* chamber.

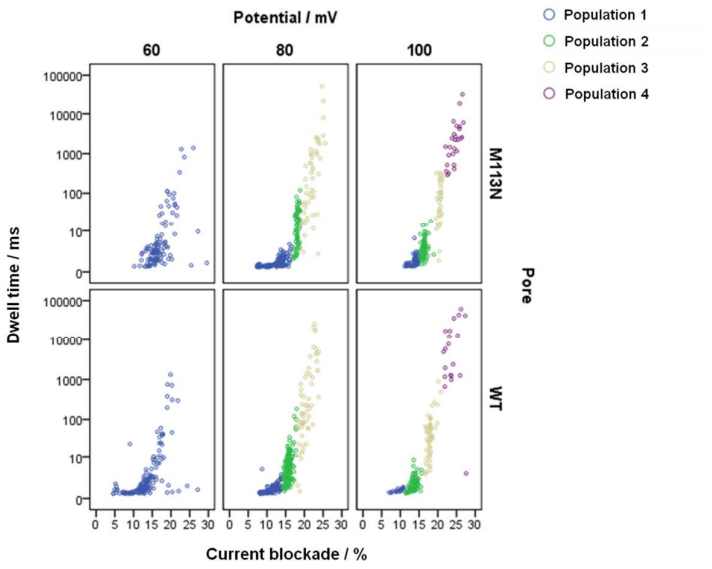

Figure S11. Scatter plots of blockade duration (dwell time) *versus* the current blockade for the interaction of MPSA NPs with the M113N mutant nanopore and with the WT-αHL nanopore. The experiments were performed at different applied transmembrane potentials in 2 M KCl buffered with 10 mM HEPES (pH 8.0), in the presence of 10 μg mL^{-1} MPSA NPs added to the *cis* chamber.

Table S1. Current blockade percentage and dwell time values for the interaction of MPSA NPs with the protein nanopores and γCD. [a, b]

				Level 1			Level 2			Level 3		
Nanopore	**CD**	V_m	**Type**	**Blockade/%**	**Dwell time/ms**	***N***	**Blockade/%**	**Dwell time/ms**	***N***	**Blockade/%**	**Dwell time/ms**	***N***
M113N	γCD	40	A	17.0	1.0	33	65.1	122.7	427	89.1	0.5	115
		60	A	15.6	1.8	500	66.1	101.4	690	81.3	0.5	186
			B	23.6	399.6	13	66.3	128.6	13	72.8	24.2	13
			C	32.7	312.0	14	65.9	199.2	2	75.9	105.3	14
		80	A	16.2	1.8	1306	66.7	68.1	539	80.7	0.5	76
			B	24.3	375.1	136	66.7	56.0	136	73.4	6.5	136
			C	35.4	354.6	170	66.7	98.1	20	77.5	183.3	170
			D	22.3	161.3	10	66.6	111.0	10			
		100	A	16.1	2.8	1028	67.1	47.6	146	75.3	0.5	16
			B	26.2	390.4	205	67.1	41.2	204	74.2	6.8	205
			C	35.9	299.5	258	67.1	58.6	44	78.3	106.1	258
			D	21.3	148.5	56	67.2	49.5	56			

Table S1. (cont.)

				Level 1			Level 2			Level 3		
Nanopore	**CD**	V_m	**Type**	**Blockade/ %**	**Dwell time/ms**	***N***	**Blockade/ %**	**Dwell time/ms**	***N***	**Blockade/ %**	**Dwell time/ms**	***N***
WT-αHL	γCD	40	A	11.8	0.6	43	66.7	145.1	525	87.2	0.5	309
		60	A	13.7	1.0	393	67.6	117.1	1217	86.4	0.5	480
			B	20.8	354.8	10	67.7	50.8	10	74.2	4.5	10
			C	25.1	1210.6	3	67.8	198.3	1	75.5	273.0	3
			D	17.9	70.2	2	68.6	13.0	2			
		80	A	15.9	3.1	1230	68.3	87.6	1057	81.5	0.5	375
			B	22.9	284.9	88	68.3	74.1	88	74.7	8.5	88
			C	36.2	410.8	177	68.2	83.9	16	80.2	299.0	177
			D	20.7	126.5	16	68.2	198.7	16			
		100	A	15.0	2.1	1808	68.8	68.8	437	80.8	0.5	109
			B	24.5	369.1	231	68.8	65.0	230	75.6	6.5	231
			C	36.9	351.9	304	68.8	69.3	46	80.6	318.0	304
			D	20.5	123.7	45	68.9	74.6	45			

[a]Experiments were performed in 2 M KCl, 10 mM HEPES (pH 8.0), in the presence of 20 μM γCD added to the *trans*-side and 10 μg mL^{-1} MPSA NPs added to the *cis* side. [b]Current blockade percentage = $100 \times (I_O - I_B)/I_O$, where I_O is the current of the open nanopore, and I_B is the current of the blocked nanopore. Current blockade and dwell time values are expressed as the median of *N* individual events, in n = 4-10 recordings obtained from 4 independent experiments.[38, 39]

Table S2. Ionic current, current blockade and dwell time values for the interaction of γCD with protein nanopores [a, b]

V (mV)	I_O (pA)	I_B (pA)	Blockade (%)	Dwell time (ms)	N
M113N mutant nanopore					
+100	191 ±5	64 ± 1	66.7 ± 0.6	18.5	35
+80	151 ± 4	50 ± 2	66.7 ± 0.5	61.2	104
+60	111 ± 2	38 ± 1	65.8 ± 1.0	50.0	81
+40	74 ± 2	25 ± 1	65.6 ± 0.1	267.8	24
-60	-94 ± 5	-39 ± 1	58.9 ± 0.4	70.8	69
-80	-119 ± 3	-51 ± 1	57.5 ± 0.5	306.3	90
-100	-144 ± 3	-64 ± 2	56.3 ± 1.1	157.9	33
WT-αHL nanopore					
+100	196 ± 3	61 ± 3	69.0 ± 0.4	80.1	93
+80	154 ± 2	49 ± 2	68.4 ± 0.3	76.5	137
+60	113 ± 1	36 ± 2	68.0 ± 0.6	98.0	136
+40	74 ± 1	25 ± 2	66.5 ± 0.6	165.5	56
-60	-99 ± 1	-36 ± 1	61.5 ± 0.5	475.5	28
-80	-128 ± 2	-49 ± 1	60.0 ± 0.2	534.7	49
-100	-158 ± 2	-61 ± 2	58.8 ± 0.0	216.3	22

[a]Experiments were performed in 2 M KCl, 10 mM HEPES (pH 8.0), in the presence of γCD, added to the *trans* side, at a concentration of 20 μM. [b]Current blockade percentage = 100 × (I_O − I_B)/I_O, where I_O is the current recorded during the open nanopore state, and I_B is the current recorded when the nanopore is (partially) blocked. Current and current blockade values are expressed as the mean ± standard deviation. Dwell time values are the median of N individual events, in n = 4-9 independent experiments.[30, 31]

Table S3. Diameter of WT-αHL and M113N β barrels (in nm), as determined from 7AHL[13] (wild-type) and 3M4D[4] (M113N mutant) using the PyMOL software[22] measurement wizard.

Nanopore	**Lys147**	**Met113**	**Leu135**	**Asn139**
WT	1.44 ± 0.09	1.59 ± 0.05	1.67 ± 0.06	2.06 ± 0.03
Nanopore	**Lys147**	**Met113Asn**	**Leu135**	**Asn139**
M113N	1.18 ± 0.01	1.58 ± 0.02	1.62 ± 0.04	1.96 ± 0.04

Table S4. Current blockade percentage and dwell time (τ_{off}) values for the interaction of MPSA NPs with the M113N mutant and WT-αHL nanopores.[a,b]

Nanopore	**M113N**			**WT-αHL**		
	%Blockade	**τ_{off} / ms**	***N***	**%Blockade**	**τ_{off} / ms**	***N***
+60 mV	17.08 ± 3.3	2.4	106	13.3 ± 4.1	1.0	144
+80 mV	12.6 ± 2.2	0.6	156	11.0 ± 1.5	0.5	155
	18.1 ± 0.5	11.2	63	15.8 ± 0.8	5.3	135
	22.1 ± 1.7	274.2	52	20.64 ± 1.7	152.8	61
+100 mV	13.7 ± 0.9	0.7	61	9.4 ± 1.2	0.6	18
	16.4 ± 0.6	2.8	65	13.6 ± 1.0	1.6	65
	20.5 ± 0.4	73.9	35	17.9 ± 0.9	38.9	52
	24.5 ± 1.4	2216.4	26	23.9 ± 1.9	5407.2	20

[a]Experiments were performed at applied potentials of +40 mV, +60 mV, +80mV, and +100 mV in 2 M KCl, 10 mM HEPES (pH 8.0), in the presence of MPSA NPs added to the *cis* side, at a final concentration of 10 μg mL^{-1}. [b]Current blockade percentage = $100 \times (I_O - I_B)/I_O$, where I_O is the ionic current measured for the open nanopore, and I_B is the ionic current measured for the blocked nanopore. Open nanopore current and current blockade values are expressed as the mean ± standard deviation and dwell time (τ_{off}) values are expressed as the median of *N* individual events, in n = 4-5 independent experiments.[30, 31]

Table S5. Pearson correlation coefficients for the relationship between the current blockade and the dwell time of the different populations observed during the interaction of MPSA NPs with the M113N mutant and WT-αHL nanopores.

		Current blockade *versus* dwell time populations			
Nanopore	**Potential**	**1**	**2**	**3**	**4**
M113N	**+60 mV**	0.431**			
	+80 mV	0.591**	0.371**	0.393**	
	+100 mV	0.257*	0.282*	0.332**	0.508**
WT	**+60 mV**	0.333**			
	+80 mV	0.453**	0.511**	0.499**	
	+100 mV	0.809**	0.323**	0.673**	0.484**

** Correlation is significant at the 0.01 level.* Correlation is significant at the 0.05 level.

References

1. Gu, L. Q.; Braha, O.; Conlan, S.; Cheley, S.; Bayley, H. Stochastic Sensing of Organic Analytes by a Pore-Forming Protein Containing a Molecular Adapter. *Nature* **1999**, *398*, 686-690.

2. Bayley, H.; Jayasinghe, L. Functional Engineered Channels and Pores (Review). *Molec. Membrane Biol.* **2004**, *21*, 209-220.

3. Gu, L. Q.; Cheley, S.; Bayley, H. Prolonged Residence Time of a Noncovalent Molecular Adapter, beta-Cyclodextrin, Within the Lumen of Mutant alpha-Hemolysin Pores. *J. Gen. Physiol.* **2001**, *118*, 481-494.

4. Banerjee, A.; Mikhailova, E.; Cheley, S.; Gu, L. Q.; Montoya, M.; Nagaoka, Y.; Gouaux, E.; Bayley, H. Molecular Bases of Cyclodextrin Adapter Interactions with Engineered Protein Nanopores. *Proc. Natl. Acad. Sci. USA* **2010**, *107*, 8165-8170.

5. Menestrina, G. Ionic Channels Formed by Staphylococcus aureus alpha-Toxin: Voltage-Dependent Inhibition by Divalent and Trivalent Cations. *J. Membr. Biol.* **1986**, *90*, 177-190.

6. Egwolf, B.; Luo, Y.; Walters, D. E.; Roux, B. Ion Selectivity of alpha-Hemolysin with beta-Cyclodextrin Adapter. II. Multi-Ion Effects Studied with Grand Canonical Monte Carlo/Brownian Dynamics Simulations. *J. Phys. Chem. B* **2010**, *114*, 2901-2909.

7. Gu, L. Q.; Bayley, H. Interaction of the Noncovalent Molecular Adapter, beta-Cyclodextrin, with the Staphylococcal alpha-Hemolysin Pore. *Biophys. J.* **2000**, *79*, 1967-1975.

8. Li, W.-W.; Claridge, T. D. W.; Li, Q.; Wormald, M. R.; Davis, B. G.; Bayley, H. Tuning the Cavity of Cyclodextrins: Altered Sugar Adaptors in Protein Pores. *J. Am. Chem. Soc.* **2011**, *133*, 1987-2001.

9. Bhattacharya, S.; Muzard, J.; Payet, L.; Mathé, J.; Bockelmann, U.; Aksimentiev, A.; Viasnoff, V. Rectification of the Current in α-Hemolysin Pore Depends on the Cation Type: The Alkali Series Probed by Molecular Dynamics Simulations and Experiments. *J. Phys. Chem. C* **2011**, *115*, 4255-4264.

10. Luo, Y.; Egwolf, B.; Walters, D. E.; Roux, B. Ion Selectivity of alpha-Hemolysin with a beta-Cyclodextrin Adapter. I. Single Ion Potential of Mean Force and Diffusion Coefficient. *J. Phys. Chem. B* **2010**, *114*, 952-958.

11. Gu, L. Q.; Dalla Serra, M.; Vincent, J. B.; Vigh, G.; Cheley, S.; Braha, O.; Bayley, H. Reversal of Charge Selectivity in Transmembrane Protein Pores by using Noncovalent Molecular Adapters. *Proc. Natl. Acad. Sci. USA* **2000**, *97*, 3959-3964.

12. Kienker, P. K.; Lear, J. D. Charge Selectivity of the Designed Uncharged Peptide Ion Channel Ac-(LSSLLSL)3-CONH2. *Biophys. J.* **1995**, *68*, 1347-1358.

13. Song, L. Z.; Hobaugh, M. R.; Shustak, C.; Cheley, S.; Bayley, H.; Gouaux, J. E. Structure of Staphylococcal alpha-Hemolysin, a Heptameric Transmembrane Pore. *Science* **1996**, *274*, 1859-1866.

14. Szejtli, J. Introduction and General Overview of Cyclodextrin Chemistry. *Chem. Rev.* **1998**, *98*, 1743-1754.

15. Saenger, W.; Jacob, J.; Gessler, K.; Steiner, T.; Hoffmann, D.; Sanbe, H.; Koizumi, K.; Smith, S. M.; Takaha, T. Structures of the Common Cyclodextrins and Their Larger Analogues Beyond the Doughnut. *Chem. Rev.***1998**, *98*, 1787-1802.

16. Asandei, A.; Apetrei, A.; Luchian, T. Uni-Molecular Detection and Quantification of Selected β-Lactam Antibiotics with a Hybrid α-Hemolysin Protein Pore. *J. Mol. Recogn.* **2011**, *24*, 199-207.

17. Misakian, M.; Kasianowicz, J. J. Electrostatic Influence on Ion Transport through the αHL Channel. *J. Membr. Biol.* **2003**, *195*, 137-146.

18. Sa, N.; Baker, L. A. Rectification of Nanopores at Surfaces. *J. Am. Chem. Soc.* **2011**, *133*, 10398-10401.

19. Mantri, S.; Sapra, K. T.; Cheley, S.; Sharp, T. H.; Bayley, H. An Engineered Dimeric Protein Pore that Spans Adjacent Lipid Bilayers. *Nat. Commun.* **2013**, *4*, 1725.

20. Mamonova, T.; Kurnikova, M. Structure and Energetics of Channel-Forming Protein-Polysaccharide Complexes Inferred Via Computational Statistical Thermodynamics. *J. Phys. Chem. B* **2006**, *110*, 25091-25100.

21. Gu, L. Q.; Cheley, S.; Bayley, H. Capture of a Single Molecule in a Nanocavity. *Science* **2001**, *291*, 636-640.

22. *The PyMOL Molecular Graphics System*, Version 1.4.1; Schrödinger, LLC: 2011.

23. Asandei, A.; Mereuta, L.; Luchian, T. The Kinetics of Ampicillin Complexation by γ-Cyclodextrins. A Single Molecule Approach. *J. Phys. Chem. B* **2011**, *115*, 10173-10181.

24. Campos, E.; McVey, C. E.; Carney, R. P.; Stellacci, F.; Astier, Y.; Yates, J. Sensing Single Mixed-Monolayer Protected Gold Nanoparticles by the α-Hemolysin Nanopore. *Anal. Chem.* **2013**, *85*, 10149-10158.

25. Wang, D.; Zhao, Q.; Zoysa, R. S. S. d.; Guan, X. Detection of Nerve Agent Hydrolytes in an Engineered Nanopore. *Sensors Actuat. B: Chem.* **2009**, *139*, 440-446.

26. Rincon-Restrepo, M.; Mikhailova, E.; Bayley, H.; Maglia, G. Controlled Translocation of Individual DNA Molecules Through Protein Nanopores with Engineered Molecular Brakes. *Nano Lett.* **2011**, *11*, 746-750.

27. Pinotsis, N.; Leonidas, D. D.; Chrysina, E. D.; Oikonomakos, N. G.; Mavridis, I. M. The Binding of β- and γ-Cyclodextrins to Glycogen Phosphorylase b: Kinetic and Crystallographic Studies. *Protein Sci.* **2003**, *12*, 1914-1924.

28. Campos, E.; Asandei, A.; McVey, C. E.; Dias, J. C.; Oliveira, A. S. F.; Soares, C. M.; Luchian, T.; Astier, Y. The Role of Lys147 in the Interaction between MPSA-Gold Nanoparticles and the α-Hemolysin Nanopore. *Langmuir* **2012**, *28*, 15643-15650.

29. Jadzinsky, P. D.; Calero, G.; Ackerson, C. J.; Bushnell, D. A.; Kornberg, R. D. Structure of a Thiol Monolayer-Protected Gold Nanoparticle at 1.1 A Resolution. *Science* **2007**, *318*, 430-433.

30. Dawson, B.; Trapp, R. G. *Basic & Clinical Biostatistics*. 4 ed.; McGraw-Hill: New York, 2004.

31. Manikandan, S. Measures of Dispersion. *J. Pharmacol. Pharmacother.* **2011**, *2*, 315-316.

32. Shimazaki, H.; Shinomoto, S. A Method for Selecting the Bin Size of a Time Histogram. *Neural Comput.* **2007**, *19*, 1503-1527.

33. Bland, M. *An introduction to medical statistics*. 3rd ed.; Oxford University Press: Oxford ; New York, 2000; p xvi, 405 p.

34. Lund, A.; Lund, M. Laerd Statistics. https://statistics.laerd.com/.